Design and Evaluation of a kW-Class SMES-BES DVR System for Mitigation of Power Quality Disturbances

Zi-Xuan Zheng, Xian-Yong Xiao, Chun-Jun Huang, and Chang-Song Li
College of Electrical Engineering & Information Technology
Sichuan University
Chengdu, China
scuzzx@163.com

***Abstract*—A dynamic voltage restorer (DVR) integrated with superconducting magnetic energy storage (SMES) and battery energy storage (BES) systems is proposed and its performance is evaluated in this study. Detailed model is built and verified in PSCAD/EMTDC. The dynamic performance evaluations of the SMES-BES-based DVR applied in power quality improvements are presented. Simulation results show that the SMES-BES-based DVR has good dynamic response under different kinds of voltage sag, voltage swell and voltage harmonics. Relationships obtained from different voltage sag depths and sag phase angle are explored to suit various practical sensitive load protections with the SMES-BES-based DVR.**

Keywords- dynamic voltage restorer(DVR); superconducting magnetic energy storage (SMES); hybrid energy storage (HES), battery energy storage (BES), power quality; voltage sag.;

I. INTRODUCTION

Along with the increasing importance of high-quality power supply, power quality issue has drawn considerable attention from both utility and customers. As one of the most serious power quality problems, voltage sag is a voltage decrease event between 0.1 and 0.9 pu in rms voltage for durations of 0.5 cycles to 1 minute [1]. Many modern industries, such as semiconductor industries and chemical industries, are very sensitive to voltage sags. Voltage sags have resulted in loss of important data in digital devices or even the termination of manufacturing process, thus causing enormous economic losses [2].

Dynamic Voltage Restorer (DVR) is an effective means to suppress voltage sags, which has been widely applied for improving the power quality [3-6]. As an important part of the DVR, DC energy storage system response speed, capacity and cost together play a decisive role. Among the most energy storage systems, valve-regulated lead acid (VRLA) battery is widely used with high energy density and low price. Recently many superconducting magnetic energy storage (SMES) devices have been developed and applied in compensating voltage quality disturbances for various sensitive loads for fast response speed, high power density, long life-time and little environmental pollution [7-8]. However, due to the expensive capital costs from SMES magnets [9] and affiliated refrigeration systems [10], the state-of-the-art SMES-based power devices including DVR seem to be uneconomical compared to those equipped with conventional BES systems.

To integrate the respective merits of the SMES and BES in one DVR device, we propose a new SMES-BES HES-based DVR scheme. This paper attempts to analyze and quantify the dynamic performance of hybrid SMES-BES system for sensitive load voltage compensation under different power quality disturbances.

II. SMES-BES BASED DVR

The designed 3.2-mH/240-A GdBCO SMES magnet is used to form a laboratory HES device by integrating a 40-V/100-Ah VRLA battery. The proposed SMES-BES-based HES device aims to develop a kW-class DVR. The circuit topology and main specifications of the SMES-BES based DVR are shown in Fig. 1 and Table I. It consists superconducting magnetic energy storage (SMES), battery energy storage (BES), chopper, DC-link capacitor, voltage source converter (VSC), AC filter and series transformer. Fig. 2 shows the photograph of the 3.25mH/200A SMES magnet on a winding reel.

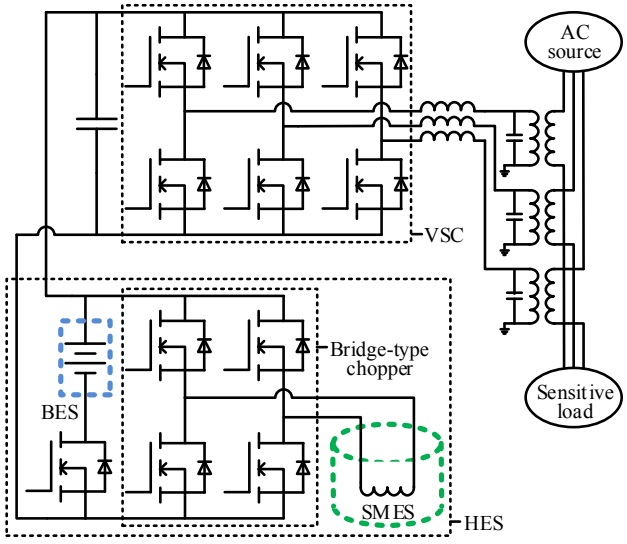

Fig. 1. Circuit topology of the SMES-BES -based DVR.

This work was supported in part by the Sichuan Science and Technology R&D Project under Grant No.2017GZ0348.

TABLE 1
MAIN SPECIFICATIONS OF THE SIMULATION SYSTEM

Item	Value
AC source voltage	380 V, 50 Hz
Sensitive load resistance	6 kW
Filter inductance	0.2 mH
Filter capacitance	0.2 mF
Transformer leak reactance	0.01 pu
Transformer turns ratio	1:10
DC-link capacitance	20 mF
DC-link rated voltage	40 V
SMES inductance	3.25 mH
SMES rated current	200 A

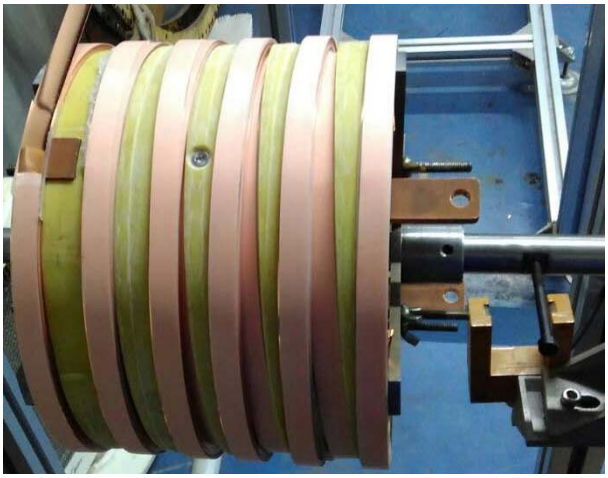

Fig. 2. Photograph of the 3.25mH/200A SMES magnet on a winding reel.

The main control system consists mainly of compensation voltage detecting strategy, VSC controlling strategy and chopper controlling strategy [11]. Through the instantaneous reactive power theory, a voltage sag can be detected with its corresponding compensation voltage signal for VSC. The hysteretic voltage controlling strategy is used for producing the pulse-width-modulation (PWM) switching signals for power electronic switches in VSC by comparing the actual compensation voltage signal with the reference value. As regards the chopper controlling strategy, it can convert the operational state of the SMES and BES between discharge mode and recharge mode by comparing the voltage of DC-link capacitor with the reference value. If the voltage of DC-link capacitor has dropped below the reference value, the chopper will be operated in discharge mode to charge the DC-link capacitor, or else will be in recharge mode.

The bridge-type chopper in Fig. 1 is formed by four MOSFETs S_1-S_4 [12,13]. This chopper has higher operational efficiency as compared to the conventional SMES chopper formed by two MOSFETs and two diodes. As for the chopper control, all the operation states are digitalized as "$S_1S_2S_3S_4$" by defining the turn-on or turn-off status of a MOSFET as "1" or "0". The charge-storage operation mode ("1010"→"0010"→"0110"→ "0010"→"1010") and the discharge-storage operation mode ("0101"→"0100"→"0110" →"0100"→"0101") correspond to the control schemes for the power absorption operation and the power compensation operation, respectively.

III. RESULTS AND DISCUSSIONS

Considering the circuit topology and main specifications of the DVR in Fig. 1 and Table I, a circuit simulation model is built in PSCAD/EMTDC. To depict the effectiveness of SMES-BES HES-based DVR in enhancing the voltage quality, four simulation conditions are considered as follows:

1) Voltage sag condition - When a symmetrical grounding fault occurs, some three-phase voltage sags are generated along the adjacent distribution lines.

2) Combined voltage sag & voltage swell condition - When a single-phase grounding fault occurs in neutral non-grounded power system, a single-phase voltage sag occurs along the grounding line and a two-phase voltage swell occurs along the other two lines.

3) Combined voltage swell & voltage sag & voltage harmonic condition - When a single-phase grounding fault occurs in neutral non-grounded power system involved with a series of nonlinear power devices, some combined voltage swell & voltage sag & voltage harmonic disturbances are generated along the adjacent distribution lines.

A. Behaviors Under Voltage Sag Condition

When a three-phase voltage sag with sag depth d_{sag} = 50% occurs from 20 ms to 120 ms, the amplitude of transient load voltage $U_R(t)$ drops rapidly from about 311 V to 176 V within half a cycle and then remains unchanged during the sag duration, as shown in Fig. 3.

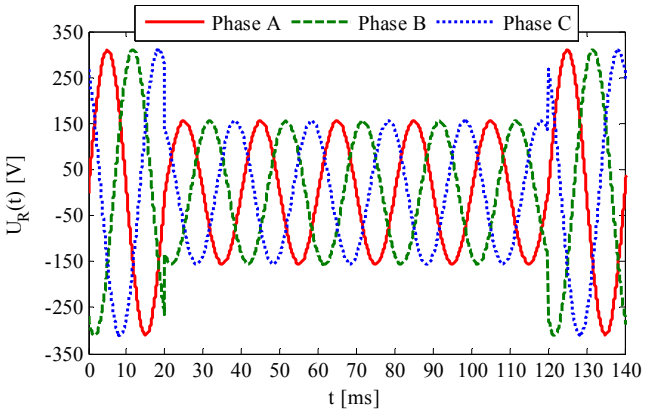

Fig. 3. Transient load voltage curves before compensation.

If the SMES-based DVR is applied, the insufficient voltage arcoss the sensitive load can be offered accurately for lasting about one and a half cycles. Accordingly, the transient load voltage after compensation in Fig. 4 is maintained at a normal level before about 50 ms. The corresponding transient power curves from the SMES is shown in Fig. 5. It can be seen that the SMES output power $P_{SMES}(t)$ drop gradually along with the time. When the amplitude of the $P_{SMES}(t)$ is greater than the required output power of 2.5 kW to the sensitive load, the transient operating state of the bridge-type chopper in Fig. 1 can be converted repeatedly between the energy discharge state and energy storage state [12,13] for releasing an average power of 2.5 kW from the SMES magnet to the sensitive load through the designed DVR.

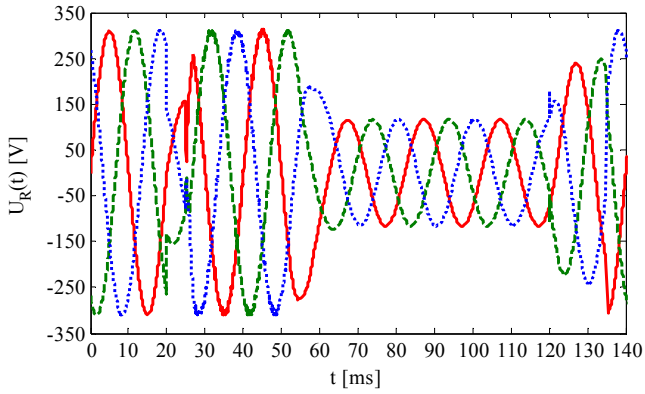

Fig. 4. Transient load voltage curves after compensation by SMES-based DVR.

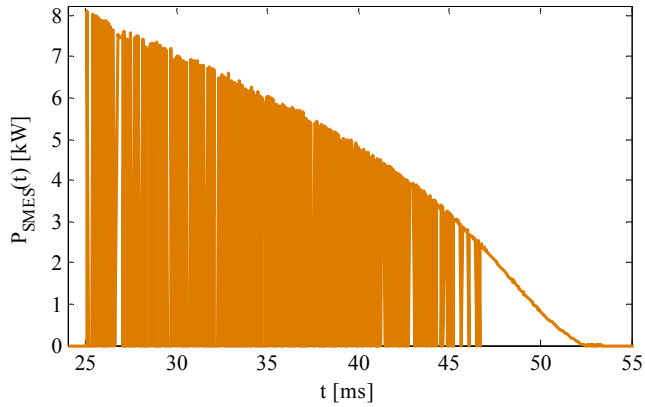

Fig. 5. Transient power curve from the SMES.

To evaluate the voltage sag compensation characteristics more accurately, a voltage compensation time duration T_{com} is defined from the time when the d_{sag} before compensation is detected to be equal to 10% to the time when the d_{sag} after compensation is reduced to 10% again. In the case of the three-phase voltage sag in Fig. 3, the RMS load voltage $U_{RMS}(t)$ drops to 342 V, i.e. 10% sag, at about 25 ms, and then the DVR starts to compensate the insufficient voltage arcoss the sensitive load. After the time when the SMES coil current drops to zero at about 52 ms, the $U_{RMS}(t)$ starts to drop gradually from 380 V to 342 V at 57 ms. This means that the T_{com} at d_{sag} = 50% is about 32 ms.

To further improve the compensation time duration, the SMES-BES-based HES scheme could be adopted in practice. In this scheme, a PNGV equivalent circuit is used to model the 40-V/100-Ah VRLA battery [14,15]. In the same case of the three-phase voltage sag in Fig. 3, the $U_{RMS}(t)$ with the HES system can also be maintained at 380 V even when the SMES coil current drops to zero at about 52 ms, as shown in Fig. 6. The compensation voltage curves from the HES-based DVR offset the insufficient voltage completely except for the period before the voltage sag is detected, as shown in Fig. 7. Therefore, the cooperate operation of the SMES system and the BES system demonstrates its significant advantage for achieving a long-time voltage sag compensation compared to the SMES-based DVR. This advantage is derived fully from the high-capacity BES system form by the 40-V/100-Ah VRLA battery.

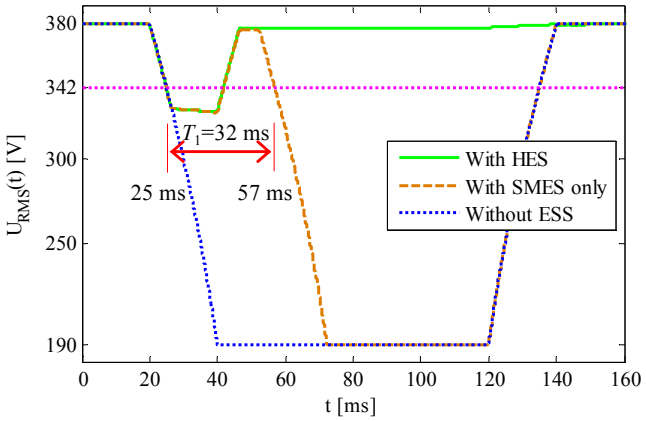

Fig. 6. RMS voltage curves after compensation by SMES-based and HES-based DVR.

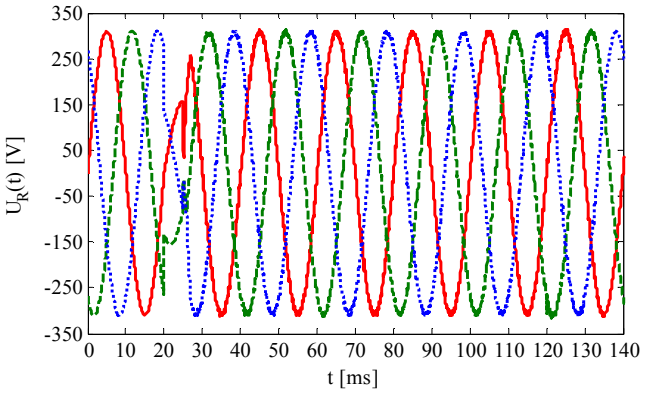

Fig. 7. Transient load voltage curves after compensation by HES-based DVR.

B. Behaviors Under Combined Voltage Swell & Voltage Sag Condition

Assuming that a single-phase grounding fault occurs from 20 ms to 120 ms in neutral non-grounded power system, thus a single-phase voltage sag (d_{sag} = 80%) is generated along the grounding line (Phase A) and a two-phase voltage swell (d_{swell} = 20%) is generated along the other two lines (Phase B, Phase C). As shown in Fig. 8, the amplitude of the transient load voltage $U_{RA}(t)$ in Phase A drops to about 43.68 V, whereas the amplitude of the transient load voltage $U_{RB}(t)$ in Phases B and C rise to about 262.9 V within half a cycle. If the SMES-BES HES-based DVR is applied, its output compensation voltage curves are with the same direction as in the insufficient load voltage component in Phase A, and also with the opposite direction as in the surplus load voltage component in Phases B and C. This means that both the insufficient and surplus load voltage components can be offset accurately for achieving near-ideal three-phase voltage curves in Fig. 9. Accordingly, the RMS load voltage in Phase A is increased from about 43.68 V to 218.9 V, and RMS load voltages in Phases B and C are decreased from about 262.9 V to 218.9 V, as shown in Fig.

10.

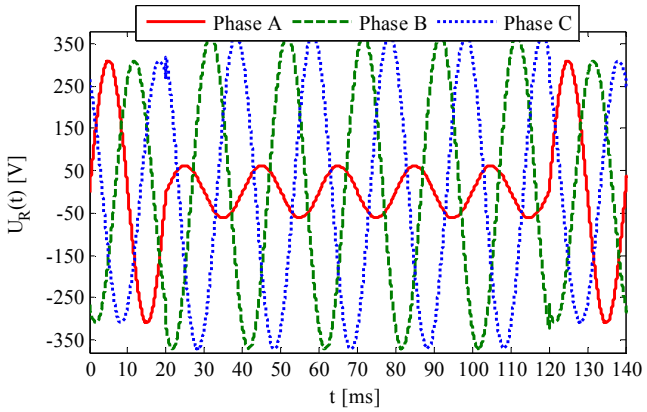

Fig. 8. Transient load voltage curves before compensation.

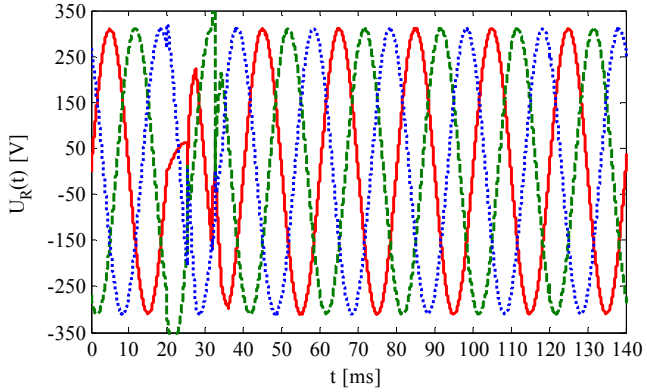

Fig. 9. Transient load voltage curves after compensation by HES-based DVR.

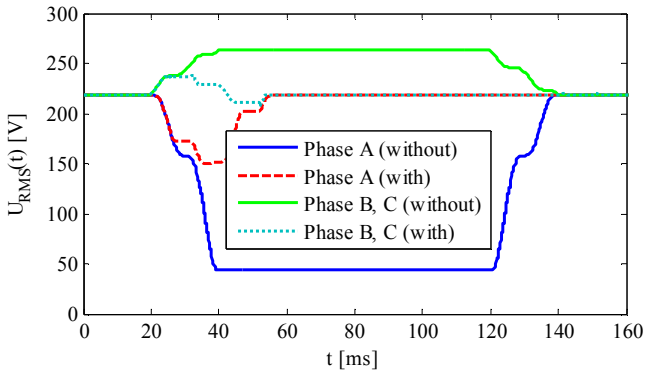

Fig. 10. RMS load voltage curves with and without the compensations by HES-based DVR.

Considering the total energy exchange requirement from three-phase lines, the surplus power is about 0.8 kW in theory. Therefore, the SMES coil is discharged and discharged repeatedly to release oscillating output power during the compensation period. as shown in Fig. 11. From the view of the whole DVR system, it releases the insufficient energy in the positive half cycle and absorbs the surplus energy in the negative half cycle. The peak releasing power and peak absorbing power $P_{DVR}(t)$ are about 1.69 kW and 0.34 kW, respectively. The RMS power difference value is almost equal to the theoretical value. Accordingly, the DC-link voltage fluctuation around 40 V also shows a oscillating trend during the whole compensation period.

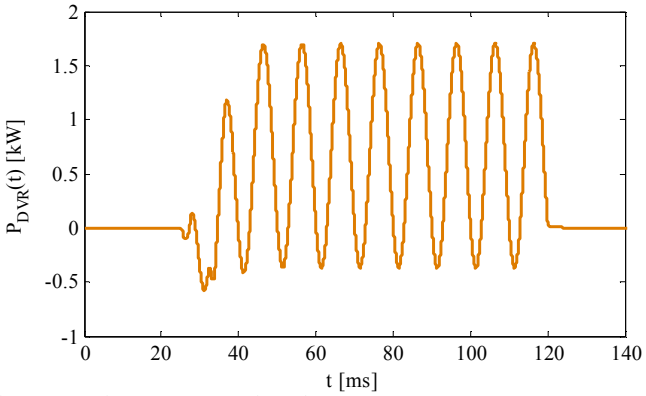

Fig. 11. Transient power curve from the DVR.

C. *Behaviors Under Combined Voltage Swell & Voltage Sag & Voltage Harmonic Condition*

Assuming that a combined voltage swell & voltage sag & voltage harmonic disturbance in Fig. 12 occurs from 20 ms to 120 ms, simulated parameters of this voltage disturbance are as follows: 1) d_{sag} = 80% in Phase A; 2) d_{swell} = 20% in Phases B and C; 3) 20% third-harmonic percentage, 20% fifth-harmonic percentage and 20% seventh-harmonic percentage in Phases A, B and C. Obvious voltage waveform distortions of the $U_R(t)$ can be found in Fig. 12 within half a cycle.

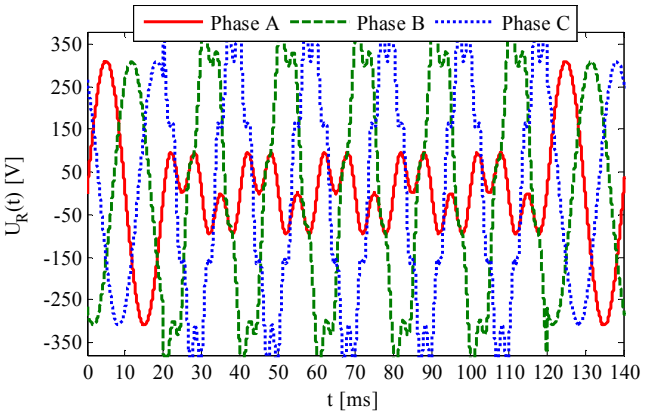

Fig. 12. Transient load voltage curves before compensation.

Although two kinds of voltage magnitude fluctuations and three kinds of voltage harmonic contents are distributed inside the three-phase voltage disturbance, the DVR can always output the required compensation voltage contents by reference to the locked real-time voltage magnitudes and phase angles before the disturbance. As a result, both the tranisent load voltage waveform in Fig. 13 and RMS load voltage waveforms in Fig. 14 are offset accurately. For the whole DVR system, the peak releasing power and peak absorbing power in Fig. 15 are about 2.06 kW and 0.64 kW, respectively.

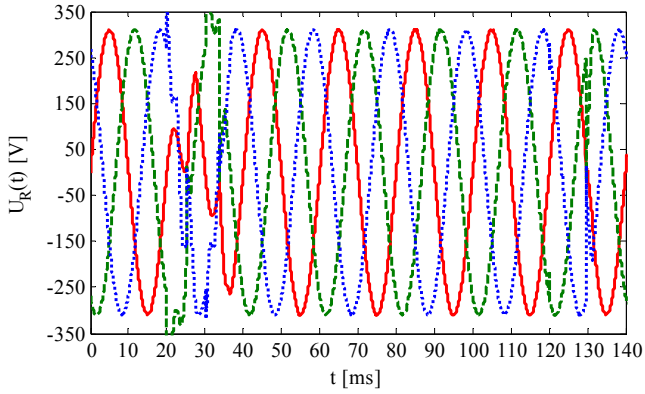

Fig. 13. Transient load voltage curves after compensation by HES-based DVR.

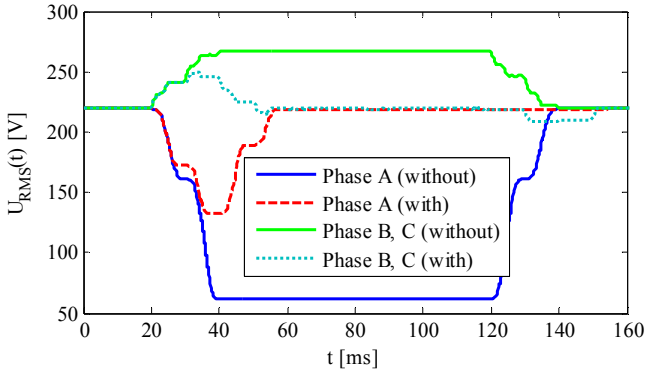

Fig. 14. RMS load voltage curves with and without the compensations by HES-based DVR.

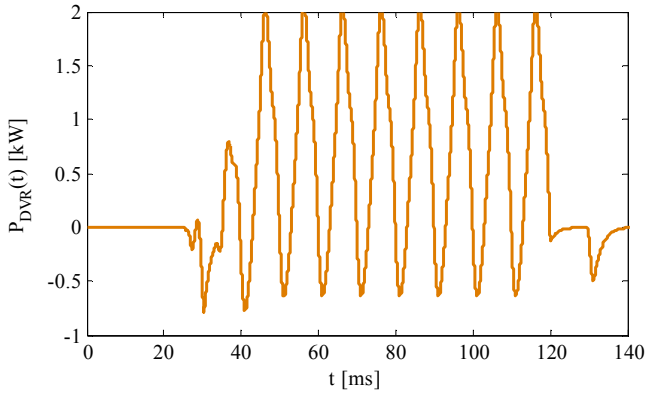

Fig. 15. Transient power curve from the DVR.

IV. Conclusions

Performance evaluations of a SMES-BES-based DVR for voltage quality compensation have been presented in this paper. The results obtained have demonstrated that the proposed system with a pre-sag compensation strategy can achieve high-precision. The introduction of medium-power high-capacity BES device extends the voltage compensation time duration significantly. For those combined voltage quality disturbances including voltage swell & voltage sag & voltage harmonic components, the pre-sag compensation strategy used in the kW-class DVR system can be used to compensate the improper voltage components exactly after symmetrical or asymmetrical voltage disturbances. Therefore, the proposed HES-based DVR concept integrated with fast-response high-power SMES unit and low-cost high-capacity BES unit can be well expected to apply in practical large-scale DVR developments and other similar applications.

References

[1] *IEEE Recommended Practice for Monitoring Electric Power Quality*, IEEE Std 1159-2009 (Revision of IEEE Std 1159-1995), Jun. 2009.

[2] G. Bonnard, "The problems posed by electrical power supply to industrial installations," *Proc. Inst. Elect. Eng. B*, vol. 132, no. 6, pp. 335-343, 1985.

[3] T. Jimichi, H. Fujita, and H. Akagi, "Design and experimentation of a dynamic voltage restorer capable of significantly reducing an energy-storage element," *IEEE Trans. Ind. Applicat.*, vol. 44, no. 3, pp. 817-825, 2008.

[4] J. D. Barros and J. F. Silva, "Multilevel optimal predictive dynamic voltage restorer," *IEEE Trans. Ind. Electron.*, vol. 57, no. 8, pp. 2747-2760, 2010.

[5] M. Moradlou, H. R. Karshenas, "Design strategy for optimum rating selection of interline DVR," *IEEE Trans. Power Del.*, vol. 26, no. 1, pp. 242-249, 2011.

[6] P. Jayaprakash, B. Singh, D. P. Kothari, *et al.*, "Control of reduced-rating dynamic voltage restorer with a battery energy storage system," *IEEE Trans. Ind. Applicat.*, vol. 50, no. 2, pp. 1295-1303, 2014.

[7] K. Shikimachi, H. Moriguchi, N. Hirano, *et al.*, "Development of MVA class HTS SMES system for bridging instantaneous voltage dips," *IEEE Trans. Appl. Supercond.*, vol. 15, no. 2, pp. 1931-1934, 2005.

[8] J. Shi, Y. J. Tang, K. Yang, *et al.*, "SMES based dynamic voltage restorer for voltage fluctuations compensation," *IEEE Trans. Appl. Supercond.*, vol. 20, no. 3, pp. 1360-1364, 2010.

[9] M. A. Green and B. P. Strauss, "The cost of superconducting magnets as a function of stored energy and design magnetic induction times the field volume," *IEEE Trans. Appl. Supercond.*, vol. 18, no. 2, pp. 248-251, 2008.

[10] S. W. Van Sciver, "Cryogenic systems for superconducting devices," *Physica C*, *Supercond.*, vol. 354, no. 1-4, pp. 129-135, 2001.

[11] Z. X. Zheng, X. Y. Xiao, C. S. Li, *et al.*, "Performance evaluation of SMES system for initial and steady voltage sag compensations," *IEEE Trans. Appl. Supercond.*, vol. 26, no. 7, pp. 5701105, 2016.

[12] J. X. Jin and X. Y. Chen, "Cooperative operation of superconducting fault-current-limiting cable and SMES systems for grounding fault protection in a LVDC network," *IEEE Trans. Ind. Applicat.*, vol. 51, no. 6, pp. 5410-5414, 2015.

[13] X. Y. Chen and J. X. Jin, "Energy efficiency analysis and energy management of a superconducting LVDC network," *IEEE Trans. Appl. Supercond.*, vol. 26, no. 7, pp. 5403205, 2016.

[14] V. H. Johnson, "Battery performance models in ADVISOR," *Journal of Power Sources*, vol. 110, no. 2, pp. 321-329, Aug. 2002.

[15] C. Q. Wang and X. M. Cheng, "A study on equivalent circuit model for VRLA battery of electric vehicle," *Annual Conference of the Society of Automotive Engineers of China*, pp. 181-184, Beijing, Oct. 20-22, 2009.